

SiGRRW: A Single-Watermark Robust Reversible Watermarking Framework with Guiding Strategy

Zikai Xu, Bin Liu, Weihai Li, Lijunxian Zhang, Nenghai Yu

{ustcxzk@mail., flowice@, whli@, ljxzhang@mail., ynh@}ustc.edu.cn

University of Science and Technology of China

Anhui, China

Abstract

Robust reversible watermarking (RRW) enables copyright protection for images while overcoming the limitation of distortion introduced by watermark itself. Current RRW schemes typically employ a two-stage framework, which fails to achieve simultaneous robustness and reversibility within a single watermarking, and functional interference between the two watermarks results in performance degradation in multiple terms such as capacity and imperceptibility. We propose SiGRRW, a single-watermark RRW framework, which is applicable to both generative models and natural images. We introduce a novel guiding strategy to generate guiding images, serving as the guidance for embedding and recovery. The watermark is reversibly embedded with the guiding residual, which can be calculated from both cover images and watermark images. The proposed framework can be deployed either as a plug-and-play watermarking layer at the output stage of generative models, or directly applied to natural images. Extensive experiments demonstrate that SiGRRW effectively enhances imperceptibility and robustness compared to existing RRW schemes while maintaining lossless recovery of cover images, with significantly higher capacity than conventional schemes.

1. Introduction

Images serve as a fundamental component of modern communication, driving exponential transmission across network platforms. However, the transmission of natural images and model-generated images via social media are faced with deliberate or unconscious copyright infringement risks, including piracy and surrogate model attacks [16, 38]. Robust watermark is an effective copyright protection technique with resistance to distortions during transmission [10, 24, 32]. And when images remain undistorted by external factors, distortions introduced by water-

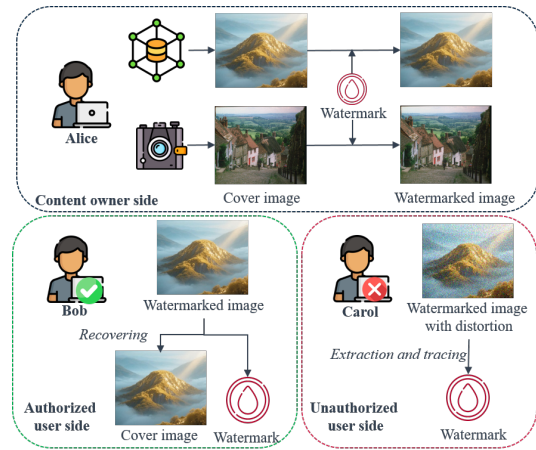


Figure 1. An application scenario of RRW

mark itself should also be considered. Any distortion of original images may compromise specific applications such as medical imaging, professional photography and deep model training [26]. Therefore, transmitted images should be losslessly recoverable by authorized users, and Robust Reversible Watermarking (RRW) has been developed to address both external and internal distortion issues [22]. One application scenario of RRW is shown in Fig. 1, where the content owner embeds watermark into the cover images generated by models or cameras, and then publishes them via the Internet. Unauthorized users may access and utilize these images, while watermark can be extracted from the images for traceability even after distortion. Authorized users can remove the watermarks to recover the original images without degradation under non-attack conditions, enabling further precision applications such as medical imaging research or model training.

Current robust reversible watermarking schemes usually employ a two-stage framework [26], achieving notable performance in both robustness and reversibility, and they outperform earlier frequency-domain feature computation approaches in various terms. The two-stage RRW is implemented by first embedding messages via a robust water-

mark, and then embedding a reversible watermark to carry auxiliary information for recovery of the robust embedding. Fundamentally, two-stage framework merely combines two distinct watermarks, and it does not constitute a genuine RRW scheme implemented with a single watermark. Compared with single-watermark schemes, such a combination inevitably degrades robustness, reduces embedding capacity, and increases computational cost. The reason is that the embedding of additional auxiliary data diminishes the overall capacity available for the intended message, and when suffering attacks, the damaged reversible watermark usually brings additional distortion into the robust one which further weakens its robustness. Moreover, existing reversible watermarking schemes mostly rely on conventional mathematical computations, which further constrain embedding capacity and imperceptibility [9].

To address the aforementioned constraints, we propose SiGRRW, a novel **Single-watermark Guided Reversible Robust Watermarking** scheme for both natural images and model-generated images, performing robust embedding and lossless recovery. We note that cover image I_o and watermarked image I_w maintain highly similar structures to preserve both visual and statistical consistency, thus identical features between them can be retrieved and utilized to guide reversible embedding. If the watermark is embedded following the guidance of identical feature representations, the resulting embedding residual becomes uniquely determined by either I_o or I_w , and can therefore be reliably computed from it. Then original image is recovered by removing the residual from I_w . We introduce a novel *guiding strategy* to ensure reversibility, where **Guider** is utilized to output identical guiding images I_g guaranteed by the similar net structure to the embedding subnet. The watermark is embedded into I_o based on the trained guiding residual, which is generated from the embedding to I_g . Later the identical guiding image and residual can be acquired by **Guider** with I_w , and the original image can be recovered losslessly by removing guiding residual from I_w . Furthermore, the incorporation of a noise layer during training facilitates enhanced robustness while maintaining reversibility.

After training, SiGRRW is free of model parameter modifications to be plug-and-play for models, and it also maintains compatibility with natural images. The main contributions are summarized as follows:

- We propose a deep-model-based robust reversible watermarking framework, and with a guiding strategy, the cover image can be perfectly recovered from the watermarked image while maintaining robustness.
- Component **Guider** is introduced to precisely generate identical guiding images from the cover image and the watermarked image. And the similar structures between the guiding subnet and the embedding subnet ensure maximal guiding consistency, while a novel adjustment

method guarantees completely identical consistency.

- We introduce a simplified noise layer, using parallel limited noise branches to enhance robustness of the watermark against various distortions.
- Extensive experiments illustrate that SiGRRW framework achieves lossless reversible recovery, large embedding capacity, high imperceptibility and robustness.

2. Related Work

2.1. Model Watermarking

Model watermarking can be categorized into two groups based on embedding methodology: pretrained watermarking and plug-and-play watermarking [31]. Pretrained ones embed watermarks during generative model training by correlating them with model parameters, while plug-and-play ones are train-free with more flexibility and lower cost.

Early pretrained-model watermarking methods primarily embed information through the training set [36], but they require retraining for each new watermark. To address this, Yu [37] later proposed integrating watermarking into the generative process. Wu [30] extended watermarking across various image processing tasks. Lin [15] proposed a CycleGAN-based scheme that jointly trains the generator with a frozen watermark decoder. With the rapid advancement of diffusion models, diffusion-based watermark has received increasing research attention [6, 7, 14, 28, 29, 34, 35]. Yang [35] proposes Gaussian Shading, proving it to be performance-lossless in diffusion model.

Plug-and-play ones append an additional layer after image generation, offering reduced training costs and enhanced portability across different model. Kou [13] proposes a Learnable Wavelet Network to balance imperceptibility and robustness. Wang [25] extends the traceability to multi-source images and minimizes the external rectangle operation. Zhang [38] proposes a deep model watermarking by adding a special task-agnostic barrier after the target model to embed a unified watermark into the output. Zhang [39] proposes a robust model watermarking based on structure consistency, further extending robustness.

2.2. Robust Reversible Watermarking

Typically, traditional reversible watermarking schemes are mainly achieved with mathematical techniques in spatial domain, such as difference expansion [23], histogram shifting [18], and prediction-error expansion [20]. Most of these schemes are incapable under distorted conditions, and RRW schemes have been developed. Early RRW schemes typically extended reversible watermarking technique from spatial domain to robust features in frequency domain [1]. While these schemes achieved robustness against specific attacks, they often struggle with scalability for complex distortions [3].

In recent years, two-stage RRW framework has gained widespread adoption and research attention. Wang [27] proposes a two-stage RRW framework based on independent embedding domains. Xiong [33] introduced a ciphertext-image RRW scheme enhancing robustness against JPEG compression and noise attacks. Tang [22] proposes a Zernike-Moment-based RRW scheme, utilizing embedding optimization and rounded error compensation to improve the imperceptibility of the watermark. Wang [26] extends the robustness of the two-stage RRW to cropping by embedding robust watermark into multiple local Zernike moments. Chen [3] developed an INN-based two-stage RRW framework that incorporates arithmetic coding and an END-based strategy for adaptive robustness under diverse distortions. Guo [9] proposed the first two-stage RRW against regeneration attacks [40] based on orthogonal moment.

3. Threat Model

We define the threat model considered for SiGRRW, which is commonly used in RRW methods. As shown in Fig. 1, the scenario involves three parties: the content owner Alice, authorized user Bob, and unauthorized user Carol.

Alice owns the copyright of images. She shares high-fidelity images over the Internet and employs watermarking to protect copyright. On one hand, she expects that unauthorized users cannot remove the watermark with common distortions to evade traceability; on the other hand, she desires that authorized users can utilize the images normally without being affected by the watermark-induced distortion.

Bob, who is authorized by Alice, can freely use the shared images. By employing `Restorer` provided by Alice, he is able to remove the watermark and perfectly reconstruct the original, watermark-free images losslessly ($\text{PSNR} = \infty$).

Carol, an unauthorized user, attempts to exploit Alice’s images without permission and evade traceability. Without access to `Restorer`, she tries to remove the watermark through common distortions such as common signal processing (CSP) or JPEG compression, or even employs regeneration-based approaches [40] to erase the watermark. She then republishes the processed images for profit.

4. Method

4.1. Overall Architecture

The overall architecture and training procedure of SiGRRW framework are shown in Fig. 2, which contains three modules with four subnets. The training of SiGRRW contains two stages, the pretraining of subnets and the collaborative training of the entire framework. After the collaborative training, three modules in Stage II pipeline require deployment in practical applications, namely the `Hider`, `Extractor` and `Restorer`, while **Dnet** serves solely as

an auxiliary training module. `Hider` performs reversible embedding of watermark wm into the cover image I_o . `Extractor` extracts watermark wm' from watermarked image I_w . `Restorer` recovers original image I'_o from I_w and wm' under the guiding strategy, and is distributed to authorized users.

The subnets of conventional watermark embedding are inspired by [38]. $\mathbf{H}(\cdot)$, $\mathbf{E}(\cdot)$, $\mathbf{D}(\cdot)$ and $\mathbf{G}(\cdot)$ denote the output of the subnets respectively in the following pages. We deploy a widely used UNet [19] structure as **Hnet** and **Gnet**. We apply CEILNet [5] structure for **Enet**, while PatchGAN [11] is applied for **Dnet**. Within the same epoch, each subnet shares the same parameters, even though it may appear at multiple positions in the training pipeline.

The core point of our scheme is to generate identical guiding images I_g s (I_g and I'_g) from either cover image I_o or watermarked image I_w , ensuring the identical residual can be calculated. To achieve this, we introduce a component **Guider** to implement guiding strategy, enabling the generation of identical I_g s and reversible recovery.

4.2. Guiding Strategy

Instead of directly embedding watermark into the cover image, we utilize a guiding image to guide watermark embedding, and the guiding image generated after extraction guides reversible recovery of the cover image. A component **Guider** is introduced to operate the guiding strategy, and it consists of a **Gnet** and a **Hnet** as shown in Fig. 2.

More explicitly, in the embedding phase, cover image I_o is input into **Guider** to generate guiding image I_g , then watermark wm is embedded into I_g with **Hnet**, and the guiding residual is calculated and transferred to I_g . As shown in Eq. (1), where $I_g = \mathbf{Guider}(I_o)$.

$$I_w = I_o + (\mathbf{H}(I_g || wm) - I_g) \quad (1)$$

In the recovery phase after extraction, **Guider** guarantees that the identical guiding image I'_g can be generated from I_w , satisfying $\mathbf{Guider}(I_o) = \mathbf{Guider}(I_w)$. Then the identical guiding residual can be acquired following the same workflow in the embedding phase, and we can reconstruct I'_o by removing the residual from I_w , as shown in Eq. (2), where $I'_g = \mathbf{Guider}(I_w)$ and wm' is the extracted watermark.

$$I'_o = I_w - (\mathbf{H}(I'_g || wm') - I'_g) \quad (2)$$

The designing of **Guider** involves two aspects: similarity comparison between I_g and I'_g , and consistency comparison of guiding images and original images. The detailed training procedure of **Guider** is stated in the following part.

Then I_g is concatenated with the watermark wm to generate a watermarked intermediate image $I_t = \mathbf{H}(I_g||wm)$. The residual of I_g and I_t is calculated and added to I_o to finish watermark embedding, as shown in Eq. (1).

I_w is input into `Extractor` to extract watermark wm' . And then proceeding to reversible recovery training. The guiding image I'_g is generated with I_w , following the same process as Eq. (6), differing only in replacing I_o with I_w . Then we compute I'_t and the guiding residual, which is identical to the embedding phase, and the recovered cover image I'_o is calculated as in Eq. (2).

The loss function in Stage II is a combination of loss functions in Stage I, as shown in Eq. (7).

$$\mathcal{L}_C = \mathcal{L}_{wm} + \lambda_3 \mathcal{L}_G \quad (7)$$

4.4. Robust Extension

The workflow above serves as a novel deep-model-based reversible watermarking framework, and it neglects to account for watermark robustness. Experimental results show that the current implementation is only robust to slight noise attacks, with detailed experimental data presented in the next section.

For robustness improving in RRW scenarios, we introduce an additional noise layer **Noise** after `Hider` during the training of Stage II to degrade watermarked images before extraction, as shown in Eq. (8).

$$wm'_{noise} = \mathbf{E}(\mathbf{Noise}(I_w)) \quad (8)$$

The noise layer consists of two parallel branches: a JPEG operation and a Gaussian filtering branch. The JPEG branch improves robustness against common distortions such as salt-and-pepper noise, crop, and JPEG compression by implicitly guiding the model to ignore high-frequency components where noise typically occurs. Besides, as noted in [2], nonlinear median filtering can be approximated as a linear combination of Gaussian filters. Consequently, Gaussian filtering branch simultaneously trains the model to resist median filtering. Furthermore, since image scaling operations exhibit spectral properties similar to Gaussian filtering and JPEG, it also extends robustness to scaling.

And another loss function ℓ_{noise} is introduced to the second term of \mathcal{L}_{wm} , as shown in Eq. (9), where ℓ_{noise} measures the L_2 norm of wm and wm'_{noise} , and λ_2 is the same weight as Eq. (4). This approach enhances robustness while preserving perfect reversibility.

$$\mathcal{L}'_{wm} = \mathcal{L}_{wm} + \lambda_2 \ell_{noise} \quad (9)$$

4.5. Reversible Recovery Analysis

The core points of SiGRRW framework are *identical guiding images generation* and *residual-guided watermarking*

embedding. We provide a comprehensive analysis of these points in this part.

Identical guiding images generation is fundamental for reversible recovery, and the cover image I_o can be exactly recovered if and only if $I_g = I'_g$ is strictly satisfied. Instead of directly using a **Gnet**, we apply **Guider**, where an additional **Hnet** is deployed after **Gnet**, to ensure identical guiding images generation. Because given multiple optimization objectives and loss functions, the model tends to output highly similar yet non-identical results, in other words, the loss function ℓ_g yields an extremely small non-zero value, while still introducing non-negligible pixel errors between I_g and I'_g : $\mathbf{G}(I_w) = \mathbf{G}(I_o) + \epsilon$, where ϵ denotes a minor non-zero error term. While removing consistency loss of **Gnet** will lead to feature degradation of I_g and thereby diminish guidance ability, which will be illustrated in the ablation experiments. So single **Gnet** is not suitable for guiding image generation.

Given similar UNet network structures, the minor error ϵ between I_g and I'_g neglected by **Gnet** will also fall below the response threshold of **Hnet**, leading both subnets to disregard these perturbations consistently. An auxiliary **Hnet** is deployed to compensate for the errors during I_g and I'_g generation, as shown in Eq. (10). In other words, the guiding image generation is a two-step process, primary image generation by **Gnet** and the final guiding image generation by **Hnet**. More precisely, during training, we set the quantization tolerance ϵ such that the $\text{MSE}(I_g, I'_g) \leq 10^{-6}$. Under this condition, the residual error can be completely eliminated by the rounding operation, making I_g s generated by **Guider** identical.

$$\mathbf{H}(\mathbf{G}(I_o)||I_{blank}) = \mathbf{H}((\mathbf{G}(I_o) + \epsilon)||I_{blank}) \quad (10)$$

Residual-guided watermarking embedding is another point of SiGRRW, the guiding residual of I_g should be also applicable for embedding wm into I_o . Notably, under the guidance of the consistency guiding loss ℓ_c , **Gnet** preserves the majority feature of the input image I , and the L_2 loss ℓ_{L_2} also constrains **Hnet** output to retain most structural information. As a result, the features representations used for watermark embedding are nearly identical between I_o and I_g , allowing the residual to serve as an effective initialization for embedding training. The collaborative training in Stage II refines embedding residual to better align with the embedding characteristics of I_o , thereby ensuring reliable watermark extraction.

5. Experiments

5.1. Basic Setup

5.1.1. Dataset

We use 4000 images from PASCAL VOC [4] and LAION-Aesthetics [21] for training, which involves both natural

Table 1. Comparison of basic performance (256^2 indicates an image of size 256×256)

Methods	PSNR	SSIM	Payloads	Reversible
CIN [17]	42.56	0.9792	30 bits	✗
MuST [25]	42.89	0.9883	30 bits	
DMIPP [38]	47.29	0.9997	256^2 bits	
IWRN [13]	41.55	0.9616	32 bits	
RRW-FoZM [8]	39.43	0.9823	128 bits	✓
RRW-PZMs [22]	39.34	0.9794	256 bits	
DRRW [3]	40.94	0.9995	256 bits	
RRWID [9]	42.48	0.9850	64 bits	
Ours	44.25	0.9923	256^2 bits	

images and generated images, and another 200 unseen images for validation. Specifically, **Hnet**, **Enet** and **Dnet** are trained on these images. The output images by **Hnet** paired with the input ones constitute the training set for **Gnet**. All the images including watermarks are resized to 256×256 , and we apply binary watermark images by default.

5.1.2. Implementation Details

We pretrain subnets **Hnet**, **Enet**, **Dnet** and **Gnet** for 50 epochs in Stage I, and collaboratively train the entire network for 50 epochs in Stage II, with a batchsize of 4. We apply Adam optimizer with the initial learning-rate = 0.002, and the learning rate decays by 0.2 if the loss does not decrease within 5 epochs. The hyperparameters are set to $(\lambda_1, \lambda_2, \lambda_3) = (10, 10, 1)$, and $\eta = 2$. We apply a JPEG branch ($QF = 50$) and a Gaussian Blur branch ($\sigma = 7$) as the Noise layer. All experiments are performed using Pytorch 2.7.1 and a NVIDIA 4090 GPU.

5.1.3. Metrics

The robustness and imperceptibility of the watermark is assessed, and we evaluate the reversibility by assessing the quality of the recovered images. PSNR and SSIM are utilized to evaluate the visual quality and imperceptibility of the watermarked images, and to validate the quality of the recovered image. For binary watermarks, we evaluate the accuracy Bit Error Ratio (BER) and $ACC = 1 - BER$ between wm and wm' , where BER represents the percentage of incorrect bits.

5.1.4. Baseline

We select baselines comprehensively, including both traditional methods and deep learning methods, natural images and model-generated images, and robust watermarking and reversible watermarking methods. And these state-of-the-art (SOTA) watermarking methods include: CIN [17], MuST [25], DMIPP [38], IWRN [13], RRW-PZMs [22], RRW-FoZM [8], DRRW [3] and RRWID[9].

5.2. Comparative Experiment

To provide an intuitive demonstration of the performance of the proposed scheme, comparative experiments are conducted against several SOTA schemes. Imperceptibility, robustness and embedding capacity are assessed in this part. 256×256 color cover images and 256×256 binary watermarks are employed for the proposed standard scheme. Considering various embedding patterns of baselines, different watermarking payloads of baselines are applied for comparison. Our framework still maintains outstanding performance even with much higher payloads.

5.2.1. Basic Comparison

Tab. 1 presents a comparative analysis of visual quality and embedding capacity across SOTA schemes under no-attack conditions. SiGRRW demonstrates outstanding PSNR and SSIM, and achieves the highest PSNR performance among RRW schemes despite much higher payloads than conventional ones, which evidences exceptional imperceptibility of our scheme. Furthermore, SiGRRW achieves the highest embedding capacity among all evaluated RRW schemes, establishing a new benchmark for high-capacity RRW.

Typically, deep-model-based watermarking schemes demonstrate superior embedding capacity and imperceptibility but lack reversibility, while conventional RRW schemes show weaker imperceptibility and the reversibility is realized without deep model. Our scheme achieves enhanced embedding capacity and imperceptibility performance while maintaining reversibility using deep model.

5.2.2. Robustness Comparison

We evaluate the robustness of our scheme against both common distortions and regeneration attacks. For common distortions, we compare SiGRRW with a series of SOTA RRW schemes that achieve strong robustness under conventional noise. For the more advanced regeneration attacks, prior work has shown that very few watermarking schemes can withstand such attacks, and the only existing RRW method resistant to regeneration is RRWID [9], although it is not SOTA against common distortions. So we conduct a dedicated comparison with RRWID under regeneration attacks.

Tab. 2 presents a comprehensive robustness comparison of RRW schemes under various common distortions. We configure parameters of the attack as follows: Gaussian Noise ($\sigma = 0.2$), Salt-and-Pepper Noise (density=0.1), Gaussian Blur (kernel = 7×7), Median Filtering (kernel = 7×7), JPEG ($QF = 50$), Scale (factor=0.5), Crop (50×50), Dropout (30%). While the robustness of the baseline two-stage schemes relies only upon the robust part, SiGRRW achieves both lossless reversibility and satisfactory robustness with a single watermark with the highest embedding payloads. For the performance of our standard method under different additional distortion parameter settings, please refer to Fig. 3.

Table 2. Comparison of robustness results on ACC of watermark extraction under common distortions

Method	Gaussian Noise	Gaussian Blur	SaltPepper	JPEG	Median Filter	Scale	Crop	Dropout
RRW-FoZM	96.05	99.99	56.03	99.99	94.10	93.11	53.48	61.95
RRW-PZMs	89.47	95.70	46.48	99.99	89.84	99.61	85.55	58.98
DRRW	99.99	99.99	99.99	99.99	99.99	99.99	99.99	99.99
Ours(standard)	99.87	99.84	99.82	99.11	97.45	99.81	95.20	99.69
Ours(256 bit)	100.00	100.00	100.00	100.00	100.00	100.00	99.91	99.90

Although DRRW shows slightly better robustness than our standard experimental setup, SiGRRW supports a substantially higher embedding capacity. When embedding 256-bit watermark, as shown in Tab. 2, our approach still attains SOTA performance.

We further evaluate the robustness of SiGRRW against VAE-based regeneration attacks. Regeneration attacks [40] built upon VAEs are highly effective at removing most watermarks designed by traditional or deep learning approaches. Since RRWID [9] is the only existing RRW scheme specifically designed to resist such attacks, we perform a direct comparison with RRWID using the same 64-bit embedding capacity and identical settings. We use the two VAEs with different parameter settings provided by Zhao [40] and apply 60 noise step. The experimental results are presented in Tab. 3, which demonstrates that SiGRRW achieves superior robustness against regeneration attacks compared to RRWID.

Table 3. BER results under regeneration attacks

VAE Type	Regen(VAE-Bmshj)		Regen(VAE-Cheng)	
	4	5	4	5
RRWID	4.90	2.94	9.77	6.17
Ours(64bit)	4.55	2.10	6.04	1.85

5.3. Diverse Experiments

5.3.1. Recovery after Distortion

Even when the watermarked image undergoes specific distortion, our scheme actively attempts to recover it to the original one. The recovered image exhibits higher fidelity to the cover image under the same distortion, effectively reducing the perceptual impact of the watermark itself in distorted conditions. Tab. 4 measures the PSNR between the recovered distorted images and the original images under the same distortion. Our scheme maintains partial reversibility under Gaussian Noise ($\sigma = 0.2$), Gaussian Blur (kernel = 5×5), Salt-and-Pepper Noise (density = 0.005) or Median Filtering (kernel = 7×7), proactively minimizing watermark induced artifacts in the distorted cover images.

While the other RRW schemes fail to achieve recovery after noise attacks, for the reversible watermark is damaged

by distortion and fails to extract auxiliary information after attacks, and the robust one is completely irreversible without auxiliary information. Moreover, the damaged reversible watermark may adversely affect the robust watermark and the cover image itself, leading to further degradation in fidelity.

Table 4. PSNR results of recovered images after distortion

	GausNoise	GausBlur	SaltPepper	Median Filter
(I_w, I_o)	40.80	42.52	20.73	42.76
(I'_o, I_o)	50.63	47.20	21.78	44.86

5.3.2. Tradeoff between Robustness and Reversibility

In certain scenarios involving severe distortion, our framework can enhance robustness with partial sacrifice of reversibility. Since the image is damaged by external distortions, lossless recovery has failed, and the proposed watermark essentially serves as a robust watermark. So we dynamically prioritize the strength of noise layer to boost watermark robustness while preserving partial reversibility. For the robustness enhanced version, we set the weight of noise layer as 5, and the strength of the simulation distortion as JPEG ($QF = 10$) and Gaussian Blur ($\sigma = 15$). As shown in Fig. 3, we can reduce the BER of the enhanced scheme in severe distortion scenarios compared with the standard one, achieving $PSNR(I_o, I_w) = 38.53$ and $PSNR(I_o, I'_o) = 56.18$.

5.4. Ablation Study

5.4.1. Ablation of Guide

We conduct ablation study on the components of **Guide**. Several PSNR values are presented in Tab. 5 to measure the influence of relevant components on performance. The absence of either **Gnet** or **Hnet** in **Guide** leads to non-negligible errors in guiding images generation as shown in Row 1, and then errors propagate into the final recovered

Table 5. PSNR of ablation experiments of Guider

	with all	w/o Hnet	w/o Gnet	w/o ℓ_c
(I_g, I'_g)	∞	64.73	77.54	∞
(I_o, I_w)	44.25	45.91	34.43	28.56
(I_o, I'_o)	∞	77.96	78.58	66.21

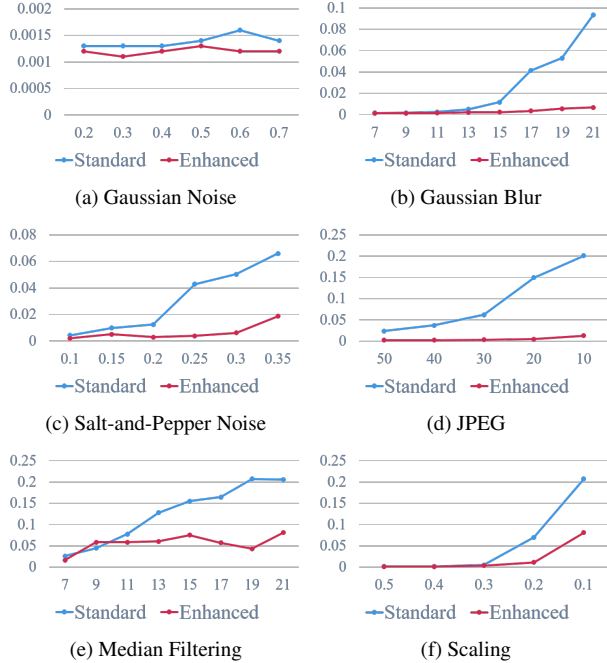


Figure 3. Robust Enhancing Results on BER

Table 6. Extraction ACC with/without Noise Layer. "0" means a blank watermark is extracted

Noise Layer	with all	w/o JPEG	w/o Filtering	w/o Noise
Gaussian Noise	99.87	99.77	99.89	99.78
Gaussian Blur	99.84	99.50	22.87	0
SaltPepper	99.82	99.54	99.29	98.32
JPEG	99.11	0	74.03	0
Median Filter	97.45	90.19	17.52	0
Scale	99.81	98.74	99.83	0
Crop	95.20	86.90	99.43	74.60
Dropout	99.69	99.42	99.26	95.59

images as shown in Row 3. So both components require mutual compensation to address their respective errors in guiding image generation.

The consistency guiding loss ℓ_c is crucial for preserving the semantic information of the cover image. As illustrated in Tab. 5, without ℓ_c , the generation of I_w exhibits feature degradation, which severely compromises imperceptibility.

5.4.2. Ablation of the Noise Layer

As shown in Tab. 6, removing either of the noise attack simulation leads to weaker robustness to certain common distortions. Training without **Noise** weakens the robustness, it can resist only limited distortion while failing against most attacks, resulting in verification failures. And removal of JPEG directly compromises robustness against JPEG compression, while removing Filtering leads to significant degradation in robustness against Gaussian blur and median filtering.

Table 7. Ablation study results of subnets

Subnet	parameter	PSNR(I_o, I_w)	SSIM	PSNR(I_o, I'_o)	BER
Hnet	w/o ℓ_{L2}	40.73	0.9885	∞	0.000
	w/o ℓ_{vgg}	39.20	0.9799	∞	0.000
	with all	44.56	0.9903	∞	0.000
Dnet	$\eta = 0$	28.33	0.8967	45.98	0.013
	$\eta = 1$	36.03	0.7940	∞	0.005
	$\eta = 2$	44.56	0.9903	∞	0.000
	$\eta = 3$	42.17	0.9801	∞	0.000
	$\eta = 5$	44.50	0.9874	96.67	0.002
	$\eta = 10$	27.37	0.8226	50.48	0.790
Gnet	layer = 4	31.62	0.8917	78.10	0.001
	layer = 5	44.56	0.9903	∞	0.000
	layer = 6	30.98	0.8941	∞	0.001

5.4.3. Ablation of Subnets

We conduct ablation study on several components of the subnets including **Hnet**, **Dnet** and **Gnet**.

The loss functions of **Hnet** during embedding training process are analyzed. Both ℓ_{L2} and ℓ_{vgg} contribute positively to the watermark imperceptibility, as illustrated in the first part of Tab. 7. Removing either loss function results in degradation of PSNR. A separate ablation study will be conducted on loss function ℓ_{adv} in the following.

The weight of **Dnet** is analyzed. As shown in the second part of Tab. 7, where η is the weight of **Dnet**. It serves as the discriminator in our framework, specializing in detecting watermark presence within images. Ablating **Dnet** during training leads to degradation in watermark imperceptibility and reversibility. Extremely high weight of **Dnet** results in excessive bias to undetectability, and induces low PSNR of the watermarked image, high BER of extracted watermark and also compromises reversibility.

The layers of **Gnet** are studied. Given 7 layers of **Hnet** for embedding, **Gnet** with 5 layers is sufficient to satisfy identical guiding images generation requirements as shown in the third part of Tab. 7. Increasing the layer count unnecessarily prolongs training costs, while insufficient layers result in failure of identical guiding images generation and reduced watermark verification success rates.

6. Conclusion

In this paper, we propose SiGRRW, a novel single-watermark Robust Reversible Watermarking (RRW) framework. Apart from conventional two-stage RRW schemes, we achieve simultaneous robustness and reversibility with only one watermark, significantly enhancing watermark imperceptibility and embedding capacity. **Guider** for guiding image generation is introduced to guide reversible watermark embedding via embedding residual. SiGRRW achieves satisfactory results against a wide range of common distortions as well as regeneration attacks. Exten-

sive experimental results demonstrate that our scheme exhibits outstanding imperceptibility and robustness performance with large capacity, while maintaining reversibility.

References

- [1] Lingling An, Xinbo Gao, Xuelong Li, Dacheng Tao, Cheng Deng, and Jie Li. Robust reversible watermarking via clustering and enhanced pixel-wise masking. *IEEE Trans. Image Process.*, 21(8):3598–3611, 2012. 2
- [2] A. Bovik, T. Huang, and D. Munson. A generalization of median filtering using linear combinations of order statistics. *IEEE Transactions on Acoustics, Speech, and Signal Processing*, 31(6):1342–1350, 1983. 5
- [3] Jiale Chen, Wei Wang, Chongyang Shi, Li Dong, Yuanman Li, and Xiping Hu. Deep robust reversible watermarking. *CoRR*, abs/2503.02490, 2025. 2, 3, 6
- [4] Mark Everingham, Luc Van Gool, Christopher K. I. Williams, John M. Winn, and Andrew Zisserman. The pascal visual object classes (VOC) challenge. *Int. J. Comput. Vis.*, 88(2):303–338, 2010. 5
- [5] Qingnan Fan, Jiaolong Yang, Gang Hua, Baoquan Chen, and David P. Wipf. A generic deep architecture for single image reflection removal and image smoothing. In *IEEE International Conference on Computer Vision, ICCV 2017, Venice, Italy, October 22-29, 2017*, pages 3258–3267. IEEE Computer Society, 2017. 3
- [6] Han Fang, Kejiang Chen, Zijin Yang, Bosen Cui, Weiming Zhang, and Ee-Chien Chang. Cosda: Enhancing the robustness of inversion-based generative image watermarking framework. In *AAAI-25, Sponsored by the Association for the Advancement of Artificial Intelligence, February 25 - March 4, 2025, Philadelphia, PA, USA*, pages 2888–2896. AAAI Press, 2025. 2
- [7] Pierre Fernandez, Guillaume Couairon, Hervé Jégou, Matthijs Douze, and Teddy Furon. The stable signature: Rooting watermarks in latent diffusion models. In *IEEE/CVF International Conference on Computer Vision, ICCV 2023, Paris, France, October 1-6, 2023*, pages 22409–22420. IEEE, 2023. 2
- [8] Dahao Fu, Xiaoyi Zhou, Liaoran Xu, Kaiyue Hou, and Xianyi Chen. Robust reversible watermarking by fractional order zernike moments and pseudo-zernike moments. *IEEE Trans. Circuits Syst. Video Technol.*, 33(12):7310–7326, 2023. 6
- [9] Bobiao Guo, Ping Ping, Fan Liu, and Feng Xu. Robust reversible watermarking with invisible distortion against VAE watermark removal. *IEEE Trans. Image Process.*, 34:6386–6401, 2025. 2, 3, 6, 7
- [10] Yiyang Guo, Ruizhe Li, Mude Hui, Hanzhong Guo, Chen Zhang, Chuangjian Cai, Le Wan, and Shangfei Wang. Freqmark: Invisible image watermarking via frequency based optimization in latent space. In *Advances in Neural Information Processing Systems 38: Annual Conference on Neural Information Processing Systems 2024, NeurIPS 2024, Vancouver, BC, Canada, December 10 - 15, 2024*, 2024. 1
- [11] Phillip Isola, Jun-Yan Zhu, Tinghui Zhou, and Alexei A. Efros. Image-to-image translation with conditional adversarial networks. In *2017 IEEE Conference on Computer Vision and Pattern Recognition, CVPR 2017, Honolulu, HI, USA, July 21-26, 2017*, pages 5967–5976. IEEE Computer Society, 2017. 3
- [12] Justin Johnson, Alexandre Alahi, and Li Fei-Fei. Perceptual losses for real-time style transfer and super-resolution. In *Computer Vision—ECCV 2016: 14th European Conference, Amsterdam, The Netherlands, October 11-14, 2016, Proceedings, Part II 14*, pages 694–711. Springer, 2016. 4
- [13] Feifei Kou, Yuhan Yao, Siyuan Yao, Jiahao Wang, Lei Shi, Yawen Li, and Xuejing Kang. IWRN: A robust blind watermarking method for artwork image copyright protection against noise attack. In *AAAI-25, Sponsored by the Association for the Advancement of Artificial Intelligence, February 25 - March 4, 2025, Philadelphia, PA, USA*, pages 370–378. AAAI Press, 2025. 2, 6
- [14] Liangqi Lei, Keke Gai, Jing Yu, Liehuang Zhu, and Qi Wu. Secure and efficient watermarking for latent diffusion models in model distribution scenarios. In *Proceedings of the Thirty-Fourth International Joint Conference on Artificial Intelligence, IJCAI 2025, Montreal, Canada, August 16-22, 2025*, pages 7473–7481. ijcai.org, 2025. 2
- [15] Dongdong Lin, Benedetta Tondi, Bin Li, and Mauro Barni. A cyclegan watermarking method for ownership verification. *IEEE Trans. Dependable Secur. Comput.*, 22(2):1040–1054, 2025. 2
- [16] Gaozhi Liu, Silu Cao, Zhenxing Qian, Xinpeng Zhang, Sheng Li, and Wanli Peng. Watermarking one for all: A robust watermarking scheme against partial image theft. In *IEEE/CVF Conference on Computer Vision and Pattern Recognition, CVPR 2025, Nashville, TN, USA, June 11-15, 2025*, pages 8225–8234. Computer Vision Foundation / IEEE, 2025. 1
- [17] Rui Ma, Mengxi Guo, Yi Hou, Fan Yang, Yuan Li, Huizhu Jia, and Xiaodong Xie. Towards blind watermarking: Combining invertible and non-invertible mechanisms. In *MM '22: The 30th ACM International Conference on Multimedia, Lisboa, Portugal, October 10 - 14, 2022*, pages 1532–1542. ACM, 2022. 6
- [18] Zhicheng Ni, Yun-Qing Shi, Nirwan Ansari, and Wei Su. Reversible data hiding. *IEEE Trans. Circuits Syst. Video Technol.*, 16(3):354–362, 2006. 2
- [19] Olaf Ronneberger, Philipp Fischer, and Thomas Brox. U-net: Convolutional networks for biomedical image segmentation. In *Medical Image Computing and Computer-Assisted Intervention - MICCAI 2015 - 18th International Conference Munich, Germany, October 5 - 9, 2015, Proceedings, Part III*, pages 234–241. Springer, 2015. 3
- [20] Vasilij Sachnev, Hyoung-Joong Kim, Jeho Nam, Suresh Sundaram, and Yun-Qing Shi. Reversible watermarking algorithm using sorting and prediction. *IEEE Trans. Circuits Syst. Video Technol.*, 19(7):989–999, 2009. 2
- [21] Christoph Schuhmann, Romain Beaumont, Richard Vencu, Cade Gordon, Ross Wightman, Mehdi Cherti, Theo Coombes, Aarush Katta, Clayton Mullis, Mitchell Wortsman, Patrick Schramowski, Srivatsa Kundurthy, Katherine Crowson, Ludwig Schmidt, Robert Kaczmarczyk, and Jenia

- Jitsev. LAION-5B: an open large-scale dataset for training next generation image-text models. In *Advances in Neural Information Processing Systems 35: Annual Conference on Neural Information Processing Systems 2022, NeurIPS 2022, New Orleans, LA, USA, November 28 - December 9, 2022*, 2022. 5
- [22] Yichao Tang, Shuai Wang, Chuntao Wang, Shijun Xiang, and Yiu-Ming Cheung. A highly robust reversible watermarking scheme using embedding optimization and rounded error compensation. *IEEE Trans. Circuits Syst. Video Technol.*, 33(4):1593–1609, 2023. 1, 3, 6
- [23] Jun Tian. Reversible data embedding using a difference expansion. *IEEE Trans. Circuits Syst. Video Technol.*, 13(8): 890–896, 2003. 2
- [24] Wenbo Wan, Jun Wang, Yunming Zhang, Jing Li, Hui Yu, and Jiande Sun. A comprehensive survey on robust image watermarking. *Neurocomputing*, 488:226–247, 2022. 1
- [25] Guanjie Wang, Zehua Ma, Chang Liu, Xi Yang, Han Fang, Weiming Zhang, and Nenghai Yu. Must: Robust image watermarking for multi-source tracing. In *Thirty-Eighth AAAI Conference on Artificial Intelligence, AAAI 2024, Thirty-Sixth Conference on Innovative Applications of Artificial Intelligence, IAAI 2024, Fourteenth Symposium on Educational Advances in Artificial Intelligence, EAAI 2024, February 20-27, 2024, Vancouver, Canada*, pages 5364–5371. AAAI Press, 2024. 2, 6
- [26] Haodong Wang, Heng Yao, Chuan Qin, and Xinpeng Zhang. When robust reversible watermarking meets cropping attacks. *IEEE Trans. Circuits Syst. Video Technol.*, 34(12): 13282–13296, 2024. 1, 3
- [27] Xiang Wang, Xiaolong Li, and Qingqi Pei. Independent embedding domain based two-stage robust reversible watermarking. *IEEE Trans. Circuits Syst. Video Technol.*, 30(8): 2406–2417, 2020. 3
- [28] Zilan Wang, Junfeng Guo, Jiacheng Zhu, Yiming Li, Heng Huang, Muhao Chen, and Zhengzhong Tu. Sleepermark: Towards robust watermark against fine-tuning text-to-image diffusion models. In *IEEE/CVF Conference on Computer Vision and Pattern Recognition, CVPR 2025, Nashville, TN, USA, June 11-15, 2025*, pages 8213–8224. Computer Vision Foundation / IEEE, 2025. 2
- [29] Yuxin Wen, John Kirchenbauer, Jonas Geiping, and Tom Goldstein. Tree-rings watermarks: Invisible fingerprints for diffusion images. In *Advances in Neural Information Processing Systems 36: Annual Conference on Neural Information Processing Systems 2023, NeurIPS 2023, New Orleans, LA, USA, December 10 - 16, 2023*, 2023. 2
- [30] Hanzhou Wu, Gen Liu, Yuwei Yao, and Xinpeng Zhang. Watermarking neural networks with watermarked images. *IEEE Trans. Circuits Syst. Video Technol.*, 31(7):2591–2601, 2021. 2
- [31] Xun Xian, Ganghua Wang, Xuan Bi, Jayanth Srinivasa, Ashish Kundu, Mingyi Hong, and Jie Ding. RAW: A robust and agile plug-and-play watermark framework for ai-generated images with provable guarantees. In *Advances in Neural Information Processing Systems 38: Annual Conference on Neural Information Processing Systems 2024, NeurIPS 2024, Vancouver, BC, Canada, December 10 - 15, 2024*, 2024. 2
- [32] Xiangli Xiao, Yushu Zhang, Zhongyun Hua, Zhihua Xia, and Jian Weng. Client-side embedding of screen-shooting resilient image watermarking. *IEEE Trans. Inf. Forensics Secur.*, 19:5357–5372, 2024. 1
- [33] Lizhi Xiong, Xiao Han, Ching-Nung Yang, and Yun-Qing Shi. Robust reversible watermarking in encrypted image with secure multi-party based on lightweight cryptography. *IEEE Trans. Circuits Syst. Video Technol.*, 32(1):75–91, 2022. 3
- [34] Yufei Yang, Song Xiao, Lixiang Li, Wenqian Dong, and Jiahui Qu. Do you steal my model? signature diffusion embedded dual-verification watermarking for protecting intellectual property of hyperspectral image classification models. In *Proceedings of the Thirty-Fourth International Joint Conference on Artificial Intelligence, IJCAI 2025, Montreal, Canada, August 16-22, 2025*, pages 2233–2241. ijcai.org, 2025. 2
- [35] Zijin Yang, Kai Zeng, Kejiang Chen, Han Fang, Weiming Zhang, and Nenghai Yu. Gaussian shading: Provable performance-lossless image watermarking for diffusion models. In *IEEE/CVF Conference on Computer Vision and Pattern Recognition, CVPR 2024, Seattle, WA, USA, June 16-22, 2024*, pages 12162–12171. IEEE, 2024. 2
- [36] Ning Yu, Vladislav Skripniuk, Sahar Abdelnabi, and Mario Fritz. Artificial fingerprinting for generative models: Rooting deepfake attribution in training data. In *2021 IEEE/CVF International Conference on Computer Vision, ICCV 2021, Montreal, QC, Canada, October 10-17, 2021*, pages 14428–14437. IEEE, 2021. 2
- [37] Ning Yu, Vladislav Skripniuk, Dingfan Chen, Larry S. Davis, and Mario Fritz. Responsible disclosure of generative models using scalable fingerprinting. In *The Tenth International Conference on Learning Representations, ICLR 2022, Virtual Event, April 25-29, 2022*. OpenReview.net, 2022. 2
- [38] Jie Zhang, Dongdong Chen, Jing Liao, Weiming Zhang, Huamin Feng, Gang Hua, and Nenghai Yu. Deep model intellectual property protection via deep watermarking. *IEEE Trans. Pattern Anal. Mach. Intell.*, 44(8):4005–4020, 2022. 1, 2, 3, 6
- [39] Jie Zhang, Dongdong Chen, Jing Liao, Zehua Ma, Han Fang, Weiming Zhang, Huamin Feng, Gang Hua, and Nenghai Yu. Robust model watermarking for image processing networks via structure consistency. *IEEE Trans. Pattern Anal. Mach. Intell.*, 46(10):6985–6992, 2024. 2
- [40] Xuandong Zhao, Kexun Zhang, Zihao Su, Saastha Vasan, Ilya Grishchenko, Christopher Kruegel, Giovanni Vigna, Yu-Xiang Wang, and Lei Li. Invisible image watermarks are provably removable using generative AI. In *Advances in Neural Information Processing Systems 38: Annual Conference on Neural Information Processing Systems 2024, NeurIPS 2024, Vancouver, BC, Canada, December 10 - 15, 2024*, 2024. 3, 7